Journal of the Brazilian Society of Mechanical Sciences and Engineering (2022) 44:298
https://doi.org/10.1007/s40430-022-03609-5

TECHNICAL PAPER

Influencing the residual stresses in tubes drawn with a floating plug by changing tool parameters

Jabbar Gattmah[1] · Fahrettin Ozturk[2,3] · Suha K. Shihab[1] · Sadettin Orhan[2]

Received: 31 October 2021 / Accepted: 6 June 2022
© The Author(s), under exclusive licence to The Brazilian Society of Mechanical Sciences and Engineering 2022

Abstract

Induced residual stresses (IRS) within tube wall produced by a floating plug drawing (FPD) is one of the vital material defects in tube drawing. Therefore, the measurements of these stresses and their correlation with manufacturing parameters are quite important in the design of the drawing tools. In the present work, DIN 17,100 St 37–2 steel tubes are pulled using the FPD process, then longitudinal and circumferential residual stresses are evaluated by the cutting method (CM). The finite element method (FEM) is also used to estimate the residual stresses in the FPD process. The influences of various tool parameters such as plug half angle, cone half angle of the die, fillet radius of the plug, and fillet radius of the die on the IRS are investigated using FEM. The results of IRS showed a good convergence between the CM and the FEM with slight differences in the values. On the other hand, the FEM results revealed that the plug half angle at 0° and the cone half angle of the die at 9° induce the minimum residual stresses compared to other angles. Further, the observation proposed that the fillet radius of the plug in the range of 0–10 mm with the fillet radius of the die in the range of 7.5–10 mm generates the compressive residual stresses which may prevent crack propagation in the tube wall.

Keywords Induced residual stresses (IRS) · Floating plug drawing (FPD) · Cutting method (CM) · Strain gage (SG) · Finite element method (FEM)

1 Introduction

Carbon steel alloys dominate tubes manufacturing that has wide industrial applications such as liquid and steam services, hydraulic tools, aerospace and vehicle pipelines, and others [1]. DIN 17,100 St 37–2 is one of the carbon steel types that extensively employed in tubes production because its good strength and corrosion resistance along with the possibility of cold working. Several techniques have been adopted to produce the tubes by calibrating the tools and workpiece to decrease the initial tube dimensions. All tube drawing processes have imperfections that affect the quality and performance of the final products [2]. The procedure of tube drawing through using a floating plug considers one of the drawing methods which apply to reduce the outer and the inner diameter as well as the thickness of the tube. The main common advantage of a floating plug drawing (FPD) as compared to other drawing processes is the ability to remove the floating plug with the control of tube orifice and the possibility to obtain long tubes [3]. Various drawing factors such as die and plug design, lubricants, drawing ratio, and material type affect the quality and surface finish of the drawn tubes [4–6]. Heidarian and Palkowski [7] built a copper-tube drawing model based on statistic technique using Minitab software for evaluating the final drawing state in terms of eccentricity that is related to the tilting angle of the die, mechanical features, drawing ratio, and tube shape. Schrek et al. [8] adopted a very small tube diameter to analyze the impact of drawing parameters on the austenitic stainless tube by simulating technique. In addition, they measured and calculated data to determine the failure (fracture) reasons in the tube wall. Chobaut et al. [9] studied

Technical Editor: Lincoln Cardoso Brandao.

✉ Jabbar Gattmah
msc_jgj_katma7@yahoo.com

[1] Department of Material Engineering, College of Engineering, University of Diyala, Baqubah, Diyala 32001, Iraq

[2] Department of Mechanical Engineering, Ankara Yildirim Beyazit University, Etlik, 06010 Kecioren, Ankara, Turkey

[3] Turkish Aerospace Industries, Inc., 06980 Kazan, Ankara, Turkey

Published online: 25 June 2022

experimentally and numerically the effect of friction and lubricant through the drawing of 316 SS tubes using a fixed plug. Further, steel tube drawing with an internal rifling was simulated by using Deform software to display the impact of the die and mandrel geometry on the tube during and after the drawing process [10, 11]. Boutenel et al. [12] determined the accuracy of the final 316 SS tube dimensions and the effect of both cone angle of the die and coefficient of friction on the pulling force. They performed models of tube drawing with and without mandrel using finite element simulation. Hosseinzadeh and Mouziraji [13] conducted the tube drawing process of pure copper using the FEM to estimate the impact of drawing factors such as tilted die angle, contact friction, stretching force on the quality of tubes. They also applied the approach of response surface methodology to choose the optimum drawing factors that produce the best quality of the final drawn square tube.

Generally, the production of tubes using a floating plug under cold forming condition generates plastic deformations because of the reduction in the tube wall and the movement of material in the forming zone in drawing direction. These plastic deformations consider one of the most important linear defects that lead to induce residual stresses (IRS) inside the wall of the final tube. The fatigue states are affected by IRS and cracks can be propagated inside the material, then the fracture occurs. Therefore, the IRS generated by drawing operations and the factors affecting require continuous and extensive investigations to reach the adoption of necessary solutions in order to reduce these stresses. Different research works have been focused on the determination of the residual stresses within the tube wall stretched by pulling methods. Ishkina et al. [14] accomplished a research to evaluate IRS within the steel tube wall type E355 during rotary swaging operation based on experimental measurements by X-ray technique and 2D-FE simulation. The thick tube was subjected to the axial extension and externally or internally was pressured to show the impact of the residual stresses on the stability in terms of the incremental response [15]. Maier et al. [16] correlated the IRS for the steel tube with the free-form bending operation factors through a movable die. They also applied a numerical approach to simulate the bending process that provides the reliability in the results—concerning to residual stresses. Gattmah et a1. [17] presented a new measurement setup for estimating the behavior of IRS in the tube wall of AISI 1010 steel through removing material layers by milling. They used strain gage type T-rosettes to measure the strain in axial and hoop directions and then residual stresses were calculated. Yan et al. [18] employed semi-destructive experimental procedures utilizing hole drilling and section technique to illustrate the impact ratio of diameter to thickness, material strength, and positions of welding on the IRS in the steel tubes. Another research concerned the measurement of generated residual stresses in the wall surface of cold-rolled AISI 321 steel pipes by removing the layers from the wall of the pipe using electrolytic etching method [19]. Kechout et al. [20] evaluated the residual stresses in composite tube walls fabricated of three-layers of PP/GEF/PP using the Crampton approach and removal technique through the measuring of the change in tube diameter when the longitudinal slot was made. Experimental and finite element procedures were implemented to validate tube drawing models, then many complex situations were performed to determine residual stresses through the pulling operation [21]. Rozenbaum et al. [22] identified IRS in 08X18H10T steel tubes that are used in heat-exchanger applications through ring procedure by vertically cutting it out of the tube to its axis. Lothhammer et al. [23] experimentally checked the IRS in the wall of the steel pipe manufactured by cold drawing based on longitudinal submerged arc welded pipe (UOE) and high-frequency welded pipes (ERW). They used the hole drilling technique to determine these stresses longitudinally and circularly. Another study recorded negative and positive residual stresses in the wall of the AISI 1010 steel tube which were calibrated by a fixed plug using both X-Ray and FEM. The different parameters, i.e., tilt angle of the die and plug, reduction in tube area, and friction coefficient numerically were considered to identify the residual stresses in axial and hoop direction [24].

It is evidently comprehended from previous investigations that there is a vital necessity to evaluate the induced residual stresses inside the tube wall with different drawing parameters. Therefore, in this study, the cutting method is adopted to measure the longitudinal residual stresses (LRS), and the circumferential residual stresses (CRS) of steel tubes utilizing the cold drawing process by a floating plug. The FEM is implemented for different models using commercially available finite element software; (ABAQUS) to exhibit the effect of plug half angle, cone half angle of the die, fillet radius of the plug, and fillet radius of the die on the IRS inside the tube wall.

2 Geometry and materials of the tools and tube

In the present study, a drawing conical die and a floating plug represent the tools used for the tube drawing process. Seamless tubes were chosen as initial tube before the forming. Figure 1a depicts the assembly of tools with the tube through the drawing operation. In the floating plug drawing (FPD), the conical die was fixed in a bench block and the initial tube was drawn by a gripped machine (drawing machine) to decrease the outer diameter. The floating plug was put within the tube freely, however, its movement remains restricted through the drawing process due to the effect of friction at the contact area between the plug and the inner

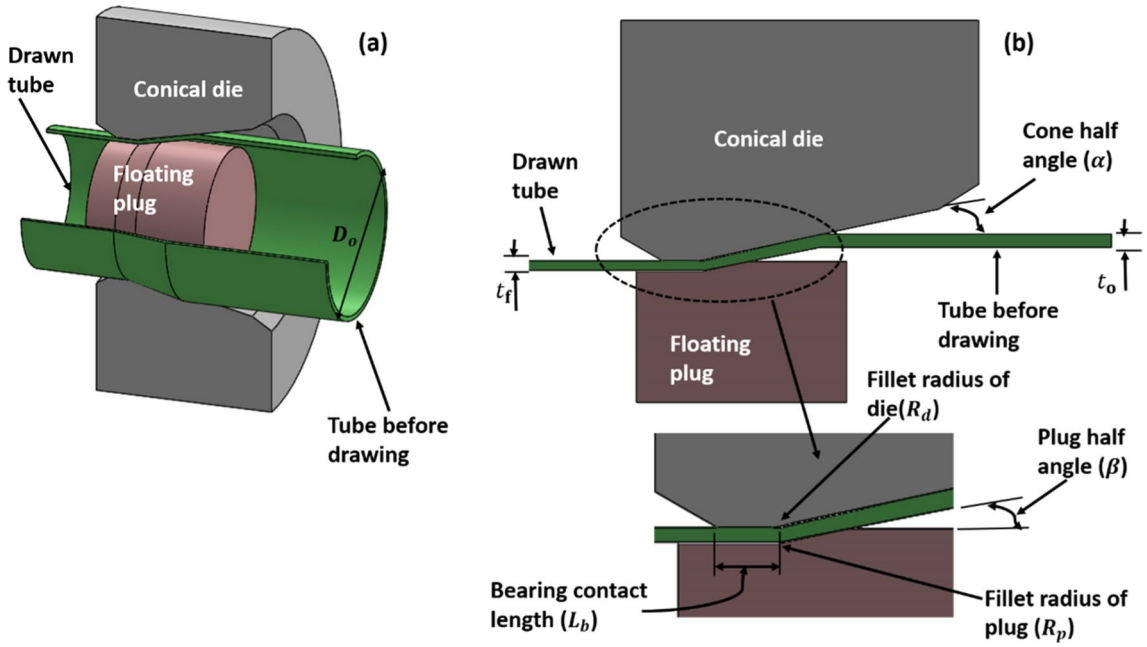


Fig. 1 Schematic representation **a** tools and tube assembly, **b** section of the FPD geometry (α, β, L_b, R_d, and R_p)

Table 1 Chemical composition of DIN 17,100 St 37–2 steel tube

Element	C	Si	Mn	P	S	Cr	Ni	Fe
DIN 17,100 St 37–2 steel wt.%	0.122	0.031	0.472	0.006	0.005	0.071	0.033	Balance

tube surfaces [25]. Figure 1b illustrates the geometry of the conical die, the floating plug as well as the tube. The conical die consists of the cone hole to form the outer diameter of the tube according to the cone half angle of the die (α). The bearing contact length (L_b) locates after forming region to ensure that the tube comes out straight while the existence of fillet radii at the internal edges of the die (R_d) reduces the impact of the sharp cone half angle through the forming process. The geometry of the floating plug has a plug half angle (β) to form the inner diameter of the tube, whereas the fillet radii of the floating plug (R_p) diminish the effect of the sharp tilted angle at the forming zone. In this experimental drawing, the cone half angle of the die ($\alpha = 9°$), bearing contact length ($L_b = 10$mm), fillet radius of the die ($R_d = 10$mm), half plug angle ($\beta = 3°$), and the fillet radius of the plug ($R_p = 5$mm) were selected. The outer diameter of the initial tube of 90mm was formed to the final diameter of 84mm, while the inner diameter was decreased from 85 to 80mm. The tube thickness of 2.5mm was considered before drawing and 2mm after drawing. The initial tube length of 2m was stretched to the final tube of 2.67m. Drawing speed ($v = 50$mm/s) was selected and mineral oil was considered for lubrication tube and tools surfaces to reduce the friction.

Tungsten carbide was chosen as the tools material (conical die and floating plug) to increase the mechanical wear resistance of the tools that occurs due to the friction between tools and tube surfaces. The Young's modulus of tungsten carbide was between 600 and 686GPa, Poisson's ratio can be taken between 0.20 and 0.22, and density represents between 15.25 and 15.88g/cm^3 [26]. Spectrographic analysis was done for the steel tube to obtain the chemical composition as given in Table 1. The mechanical features of the initial tube are summarized in Table 2.

Table 2 Mechanical features of DIN 17,100 St 37–2 steel tube

Young's modulus	206GPa	Yield Strength (Eng.)	453MPa
Density	7.95 g/cm^3	Ultimate tensile strength (Eng.)	537MPa
Poisson's ratio	0.3	Elongation to necking	30%

Tensile tests were conducted at room temperature (22 °C) employing a BZ-001/60 DCM device with a maximum force capacity of 10 t. According to the standard E8/E8M [27], three samples were prepared for the test. The determined engineering stress vs. strain curve by the tensile test is shown in Fig. 2.

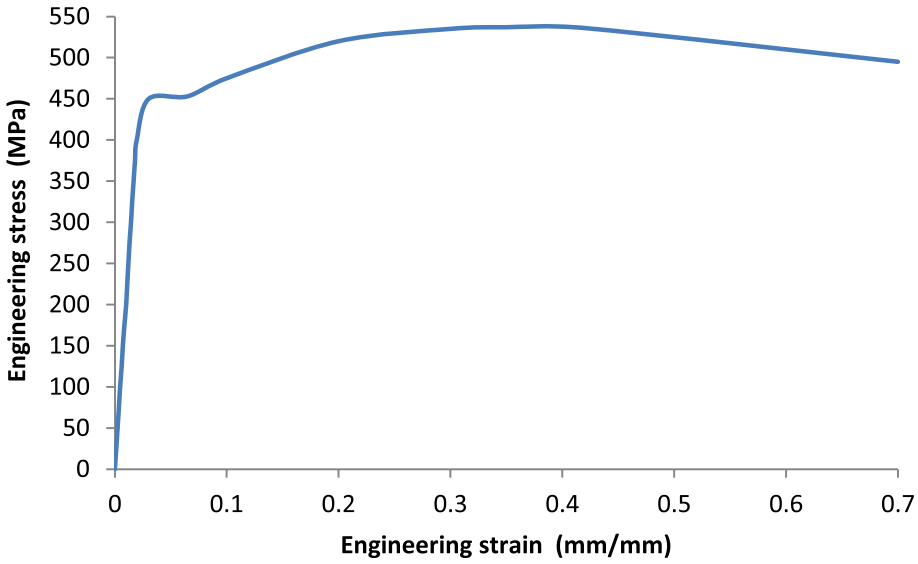


Fig. 2 Engineering stress versus strain curve of DIN 17,100 St 37–2 steel tube

3 Experimental cutting method setup for strain measurement

In this research, a cutting method (CM) was adopted to measure the strain within the tube wall using strain gages (SG). Firstly, the tube wall was cut by the saw in hoop direction to determine longitudinal residual strains, and then, the cutting of the part was performed in axial direction to identify circumferential residual strains as illustrated in Fig. 3.

The most significant task to obtain accurate measurements was the installation of three strain gages (SG1, SG2, and SG3) on the outer tube surface and determining their directions as depicted in Fig. 3. Before glueing the SG on the surface, the glued zone was carefully cleaned by removing all dust, grease, outcrops, and rust using abrasive papers. Then, M-prep conditioner was applied to clean the region area, and M-prep neutralizer was utilized to acquire free surface of obstacles completely that prevent the fixing of the SG. Adhesive type M-Bond 200 was used to stick the SG on the surface in an accurate direction based on the horizontal and vertical axes. Then, the SG was connected to the data logger for reading the strain through the cutting process. Because of using the coolant fluid to decrease the cutting temperature and to prevent thermal stress creation through the cutting, M-coat type A was selected as a material that covers and isolates the SG from any coolant leak that can be occurred. To carry out strain measurements, the SG type "CEA-06-125UN-350" at length 3mm, resistance 350 Ω, and gage factor 2.11 was adopted, while data logger (Vishay System 7000) with 32 channels was chosen. The experimental procedure was applied at the ambient temperature of 25°*C* and humidity

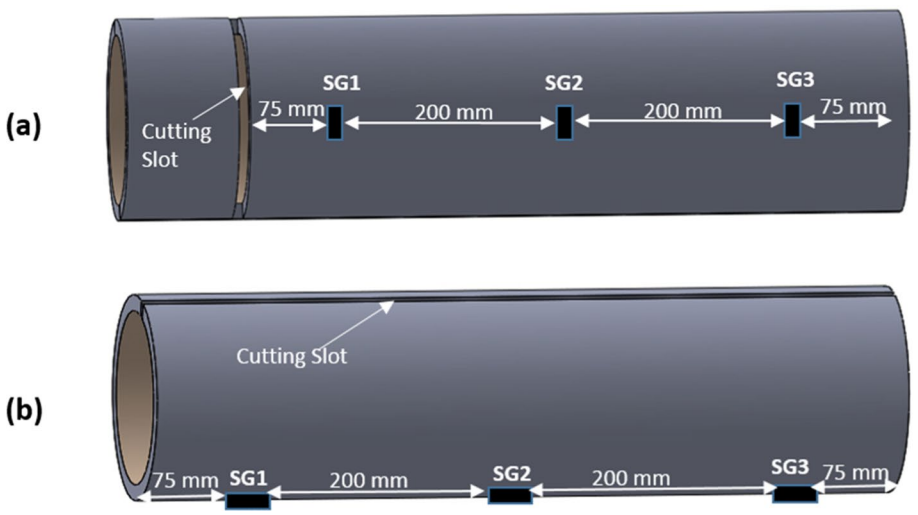


Fig.3 Cutting of the tube wall by the saw at **a** circumferential direction and **b** longitudinal direction

within the range of (30−45%). (Figure 3a and b presents the CM to measure both the longitudinal and circumferential strains, respectively, by making slots using the saw.

For obtaining the high accuracy of the measured strain values, three SG in circumferential and longitudinal directions were installed on the tube surface as depicted in Fig. 4a. The saw cutter was used to cut the tube wall, while SG senses the strains within the tube wall simultaneously as displayed in Fig. 4b and d. Then, the data logger records the strain vs. the cutting time as shown in Fig. 4c. The cutting process was achieved at the axial direction at depth of cut (2 mm) and cutting time of 60 s. The longitudinal residual stresses (LRS) and the circumferential residual stresses (CRS) were calculated based on measured strains using Hook's law [17].

4 Simulation of the IRS

In this study, simulation of the residual stresses generated during tube drawing was the main task. The walls of the steel tube as received from the supplier contain initial residual stresses inside. Therefore, the simulation of the tube drawing process was performed using ABAQUS/Standard, i.e., implicit procedure to predict the initial residual stresses for the compatibility with the experimental work, Then, the output data of these stresses in all directions were imported and applied at the beginning of the Explicit/dynamic which was an active procedure for the FPD and analysis the results [24, 28]. The input material properties of both tungsten carbide and steel were selected based on Table 2. The elastic–plastic behavior of the steel was defined according to true stress versus effective strain as shown in Fig. 5.

The FPD model was built on the base of an axisymmetric section and assuming the tube as a deformable part. The contact behavior between tools and tube surfaces was defined by two regions. One region was the friction between the inner surface of the conical die and the outer surface of the tube. Another region was the friction between the outer surface of the floating plug and the inner surface of the tube. The Coulomb friction was proposed with a coefficient of which commonly was suggested for steel drawing [29]. The element type of CAX4R was applied in the simulation. Mesh sensitivity was checked according to the relationship between a number of elements and longitudinal internal stresses (S22) and circumferential internal stresses (S33) at node in forming zone with the time step (1s). The results illustrated that the optimum mesh size was 0.6 with 528 elements when S22 and S33 equal to 257.7 and 194.4 Mpa, respectively, which indicated the start of the steady state. The number of elements for the conical die and the floating plug were adopted according to the change of the shape geometry. For the boundary condition definition, the conical die was fixed in all directions while the motion of the floating plug was

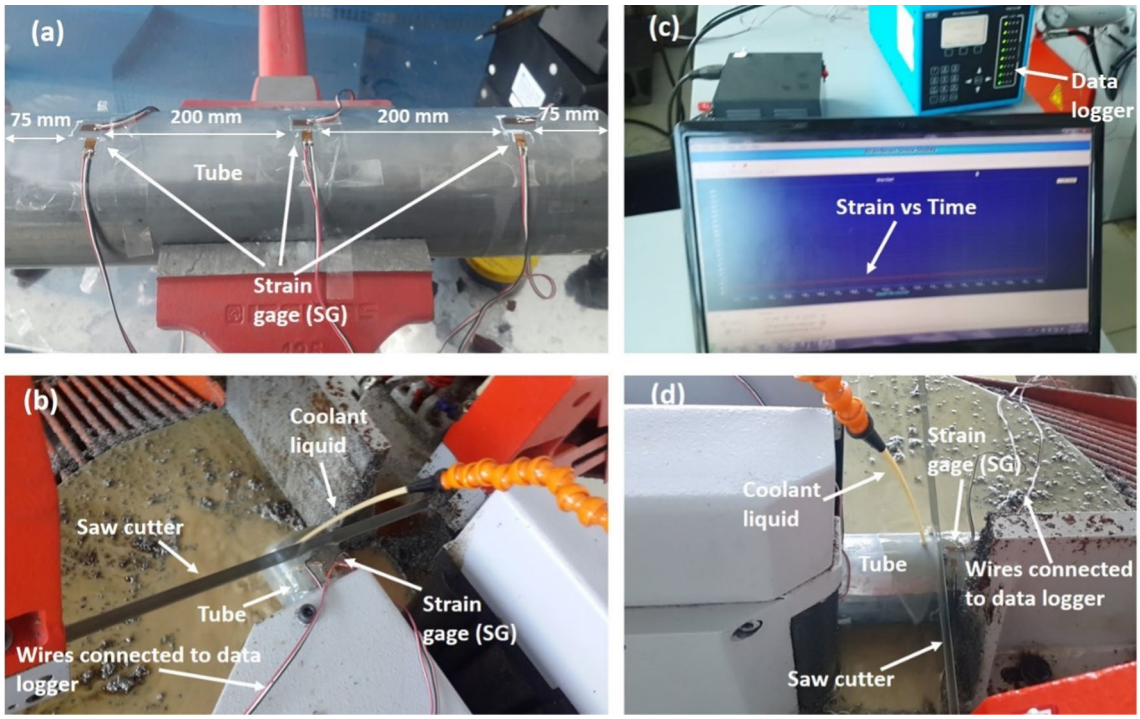


Fig. 4 Experimental setup of cutting process for the IRS measurement **a** position of the strain gages that glued on the tube surface **b** tube cutting by saw cutter with coolant liquid, **c** display the strains versus time, and **d** cutting process with coolant liquid

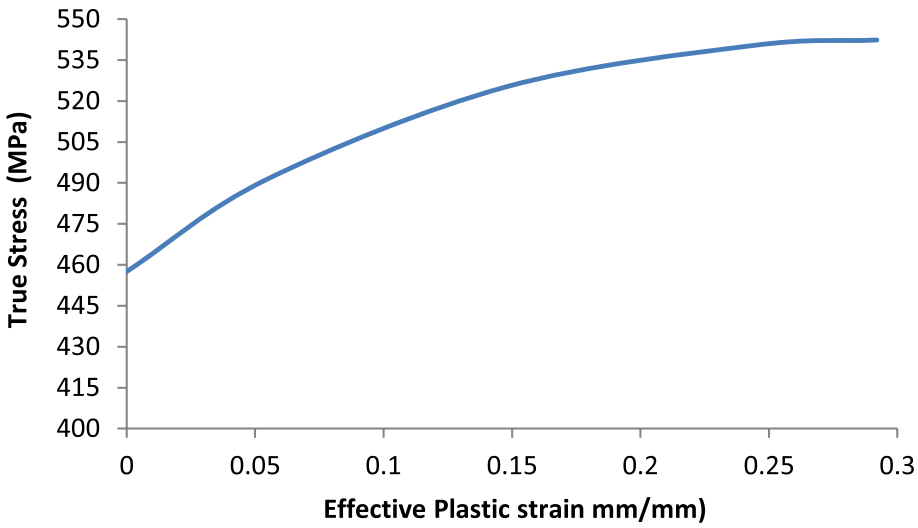


Fig. 5 True stress versus effective strain of DIN 17,100 St 37–2 steel tube

presumed at drawing direction. At β=0°, the boundary condition of the plug was given as a restricted motion in the axial direction at the tube forming to ensure that the plug does not come out with the final tube. Initial tube dimensions included outer diameter (D_o=90 mm), inner diameter (D_i=85 mm), and thickness (t_o=2.5 mm). In addition, different parameters were taken into consideration for predicting the induced residual stresses inside the final tube wall as reported in Table 3. The residual stresses were determined when the tube was fully drawn and all loads were removed.

5 Results and discussion

5.1 Residual stresses comparison using cutting and finite element methods

As mentioned in Sect. 3, the experimental procedure of the strains measurements was applied based on the CM by making the slot; then, average values of these strains along the removed material for each depth of cut were estimated. Figures 6 and 7 present the standard deviation of the longitudinal and circumferential strain values versus the depth of cut for three experimental tests. It can be noticed that the results of experiments provided good reliability with minimal errors for the experimental setup.

The experimental results of strain measurements in Figs. 7 and 8 were adopted to calculate the LRS and the CRS using Hooks law [17]. The obtained comparison of the IRS by both the CM and the FEM are revealed in Figs. 8 and 9. The selected drawing parameters were the half cone angle of the die α=9°, cone plug angle β=3°, fillet radius of the die R_d=10 mm, fillet radius of plug R_p=5 mm, and drawing velocity. It can be noticed from Fig. 8 that the LRS values are convergent in both methods (CM and FEM). In addition, the LRS values near the outer and the inner of the tube wall surfaces were negative which indicated to the compressive state. On the other hand, the LRS values at the middle area of tube thickness point out to the positive sign that refer to the tensile state. Figure 9 depicts the measurement of CRS inside the tube wall using the CM and the FEM methods. The results detected that the behavior of the CRS is similar in both experimental and numerical methods. It can also be seen from Fig. 9 that the tensile CRS locate near the outer tube surface, while the compressive CRS locate near the inner tube surface. According to the presented comparisons in Figs. 8 and 9, it can be deduced that both procedures, i.e., the CM and the FEM for IRS measurement have reliability

Table 3 Different parameters of FPD models

D_0 (*mm*) initial	T_0 (*mm*) initial	α(°)	β(°)	R_d (*mm*)	R_p (*mm*)	v (*mm*/*s*)	D_0 (*mm*) final	T_f (*mm*) final
90	2.5	5	0	0	0	50	84	2
		7	5	5	3			
		9	7	10	5			
		11	9	15	10			
		13	11	20	15			
		15	13	25	20			
		17	15	30	25			

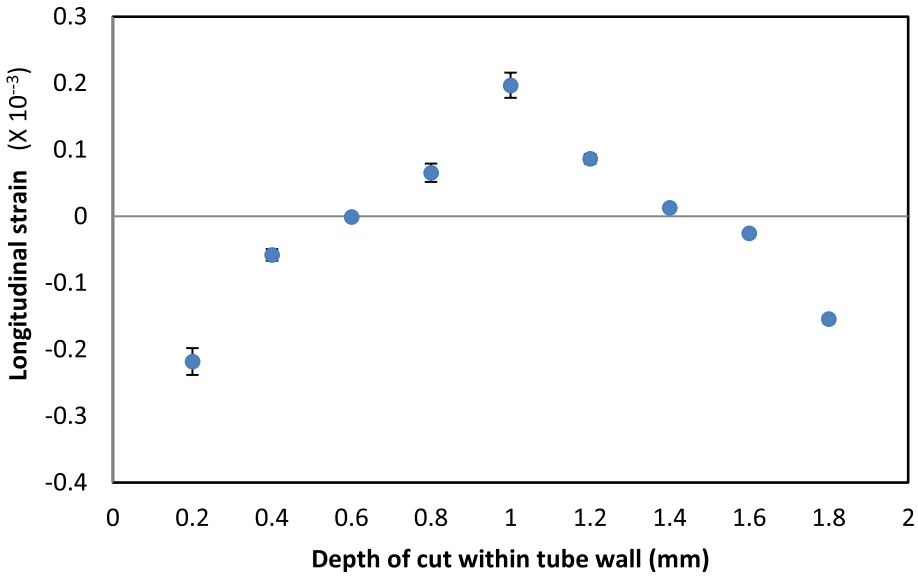


Fig. 6 Longitudinal strain versus depth of cut by the CM (0 mm = outer surface and 2 mm = inner surface)

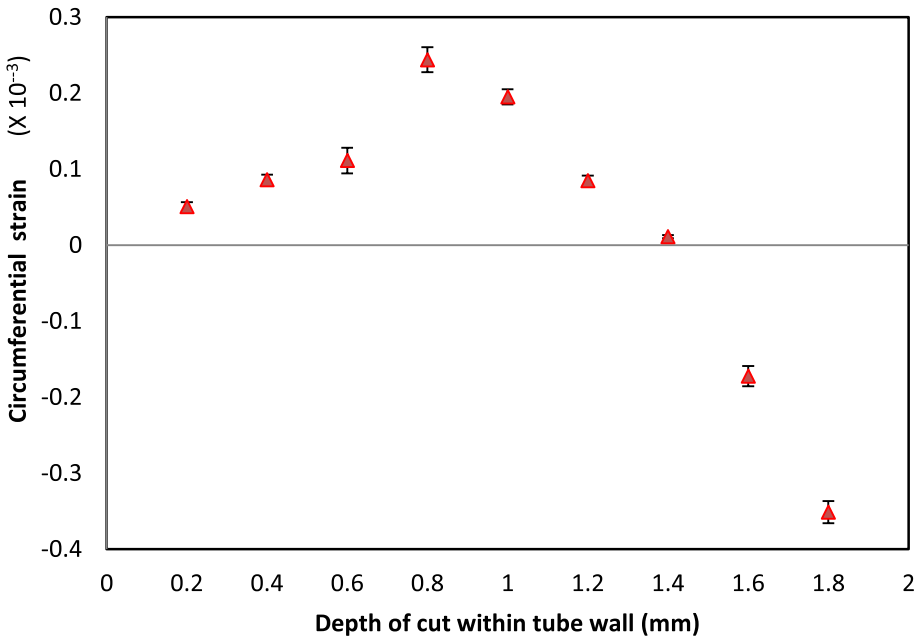


Fig. 7 Circumferential strain versus depth of cut by the CM (0 mm = outer surface and 2 mm = inner surface)

in obtained results. The figures show variation in some positions, especially at the center of the tube wall. In fact, the reason for this is that the plastic deformations are uniform deformation using the FEM, while in reality, they are nonuniform.

5.2 Stress distribution using the FEM

Figure 10a, b reveals to the type of generated stresses in both directions (longitudinal S22 and circumferential S33) during the tube drawing process at $\beta = 5°$, $\alpha = 9°$, $R_d = 10$ mm and $R_p = 0$. The contact area between tools surfaces (conical die and floating plug) and tube surfaces (the outer and the inner) through the drawing operation is clearly demonstrated in Fig. 10. The metal starts to deform due to the compression of the conical die on the outer surface of the tube at the inlet of the forming zone as presented in Fig. 10a. The tensile S22 are generated near the outer surface of the tube as a result of the die geometry (tilting cone half angle and fillet radius of the die) in a downward. However, compressive S22 are created near the inner surface because of the effect of plug geometry (plug half angle and fillet radius of the plug) that compress on the inner tube surface. Subsequently, at the outlet of the forming zone, the compressive stresses are generated at both the inner and the outer surfaces of the tube due to the effect of cone

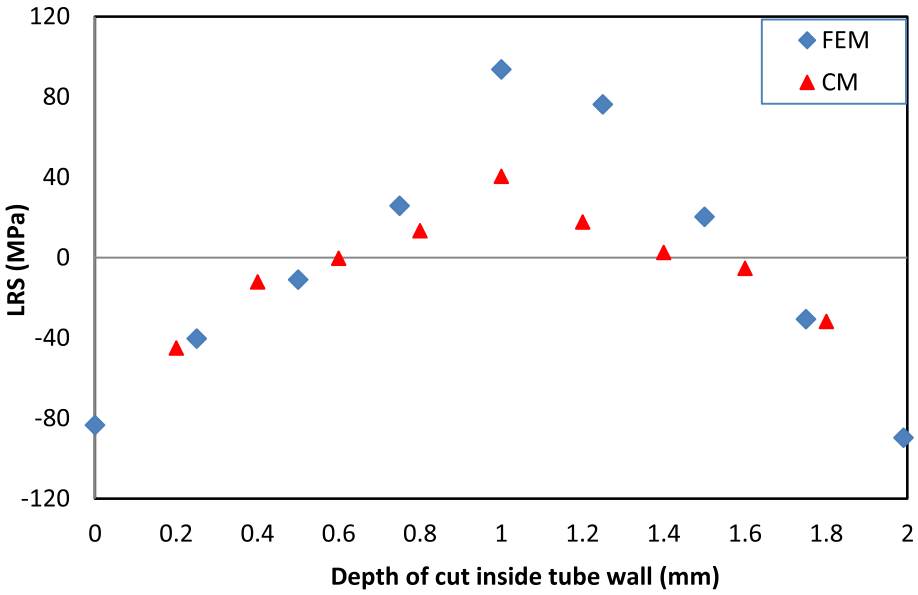


Fig. 8 Comparison results of LRS by the CM and the FEM (0 mm = outer surface and 2 mm = inner surface)

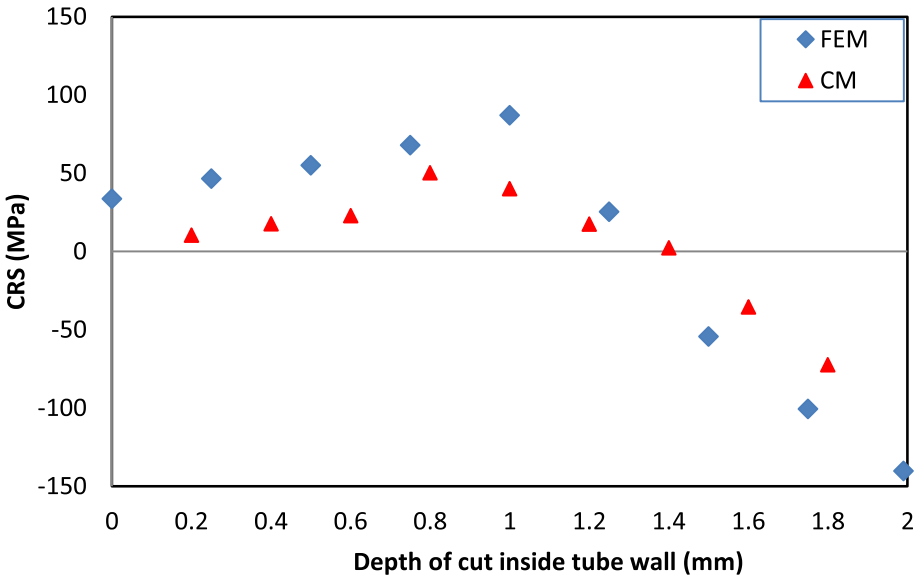


Fig. 9 Comparison results of the CRS by the CM and the FEM (0 mm = outer surface and 2 mm = inner surface)

die and plug geometry that bends tube wall upward. These results are in an agreement with the previous study [24]. It can be noticed from Fig. 10b that the S33 at the inner and the outer surfaces are in a compressive state at both forming zones (inlet and outlet). This is due to the effect of conical die and plug geometry through the drawing process that bends the tube upward in the circumferential direction as indicated in previous research [17]. It can also be observed from Fig. 10 a and b that the values of tensile S22 are higher as compared to tensile S33, while the compressive S22 are lower as compared to compressive S33. This belongs to the fact that tensile stresses augment in the axial direction and reduce in compression direction due to the drawing force effect, while compressive stresses increase in the circumferential direction (hoop direction) because of the tool's compression effect on the tube wall.

5.3 Effect of plug half angle on residual stresses

In finite element simulation, the LRS and CRS corresponding to S22 and S33 are determined at nodes along the line within the tube wall (outer, center, and inner surface), then the average value is estimated. These calculations are done when the full tube is pulled and all loads are removed.

Figures 11 and 12 present the relationship between plug half angle (β) with the LRS and the CRS, respectively, that obtained by FEM where α=9°, R_d=10 mm, and R_p=0. Figure 11 shows the LRS at three positions (the outer surface

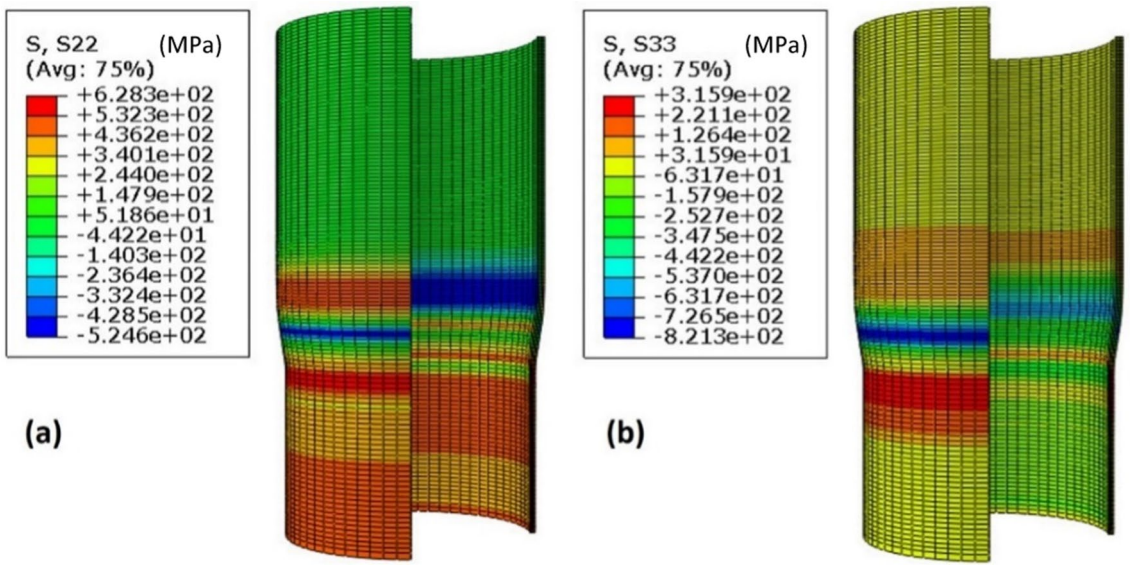


Fig. 10 Contour of the IRS during drawing process with a floating plug at **a** longitudinal direction, and **b** circumferential direction

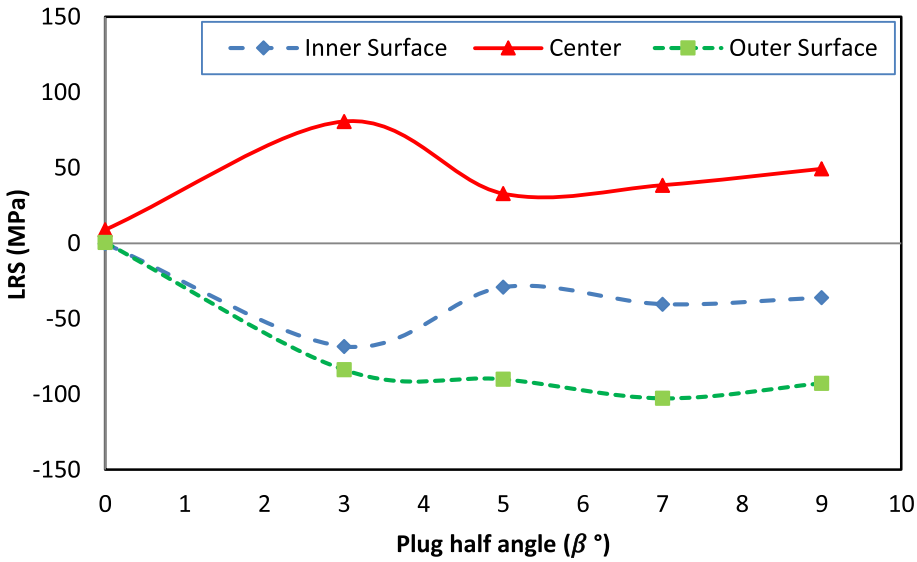


Fig. 11 Relationship between the LRS and plug half angle (β °) by FEM

of the tube, center of tube wall, and the inner surface of the tube) where compressive type is generated at the outer and the inner surfaces of the tube wall while tensile type at the center of the tube wall. Moreover, as compared to other angles, minimum values of the LRS are produced at $\beta = 0°$. As shown in Fig. 12, at the inner surface of the tube wall, the CRS are completely in a compressive state with different values of plug half angle. On the contrary, at the center of the tube wall, the CRS are in tensile type. Whereas at the outer surface of the tube wall, there is fluctuating in the type of CRS, i.e., compressive type at angles of $\beta = 0°$ and $\beta = 5$ while tensile type at other values of plug half angle. Further, it can be depicted from Figs. 11 and 12 that $\beta = 0°$ can give minimum values of the IRS in both the longitudinal and the circumferential directions because of the low slight steep of the tube wall which surges with increase in the half angle value of the plug. On the other hand, obtaining the compressive residual stresses at the inner surface of the tube plays a major role in preventing crack propagation within the drawn material [30].

5.4 Effect of cone half angle of the die on residual stresses

Based on the FEM, the effect of the cone half angle of the die (α °) on the IRS in longitudinal and circumferential

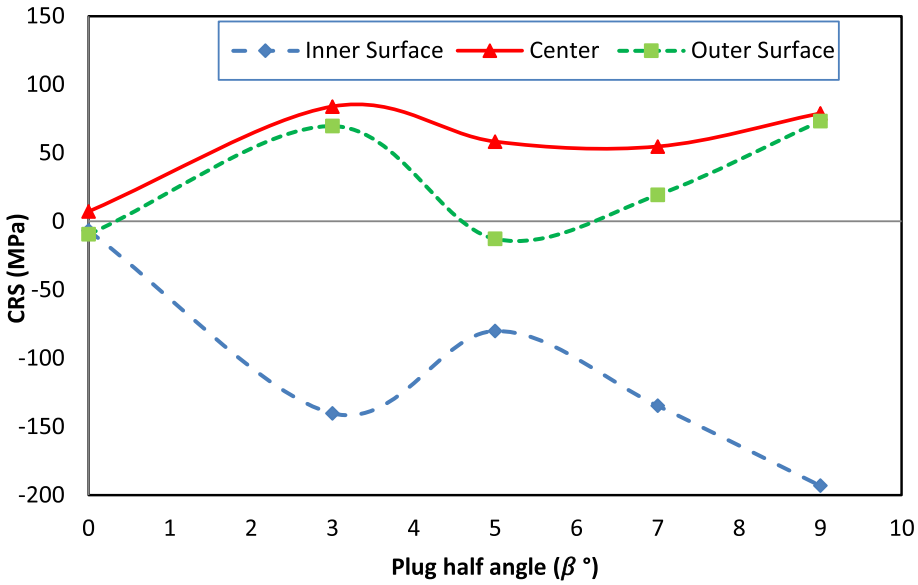


Fig. 12 Relationship between the CRS and plug half angle (β °) by FEM

directions are predicted as illustrated in Figs.13 and 14, respectively, withβ=5°, R_d=10 mm, and R_p=0. For all α, the LRS and the CRS appear in a compressive behavior at the inner and the outer surfaces of the tube, while they are in tensile state at the center of the tube wall. The minimum magnitudes of the LRS and the CRS were identified at α=9° in the three selected regions. The maximum values of the LRS and the CRS were obtained at $\alpha = 15°$ In addition, when comparing between the LRS and the CRS values in Figs. 13 and 14, it can be observed that the maximum value of the LRS was larger as compared to the maximum value of the CRS at the outer surface. On the contrary, the maximum value of CRS was higher at the inner surface. This is because the bending effect of the tube wall was downward and then upward due to steep the cone surface of the die through the drawing process as obtained by other previous research works [17, 24]. Generally, it is clear that the increase in the cone half angle of the die plays important role in determining the value and type of the IRS.

5.5 Effect of fillet radius of plug on residual stresses

According to the FEM results, the effect of fillet radius of the plug (R_p) on the LRS and the CRS are shown in Figs. 15 and 16, respectively. The parameters were used as β=5°, $\alpha = 11°$ and R_d=10 with various values of. It is clear that both the LRS and the CRS near the inner surface of the tube are compressive type while close to the center of the tube wall are tensile type. Moreover, the LRS and the CRS have different behavior at the outer surface of the tube. As

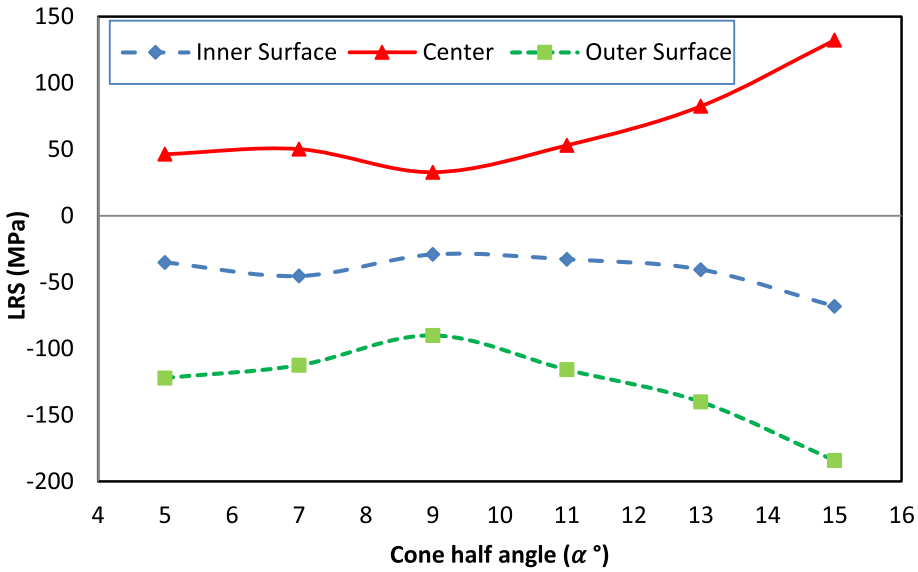


Fig. 13 Relationship between the LRS and cone half angle of the die (α °) by FEM

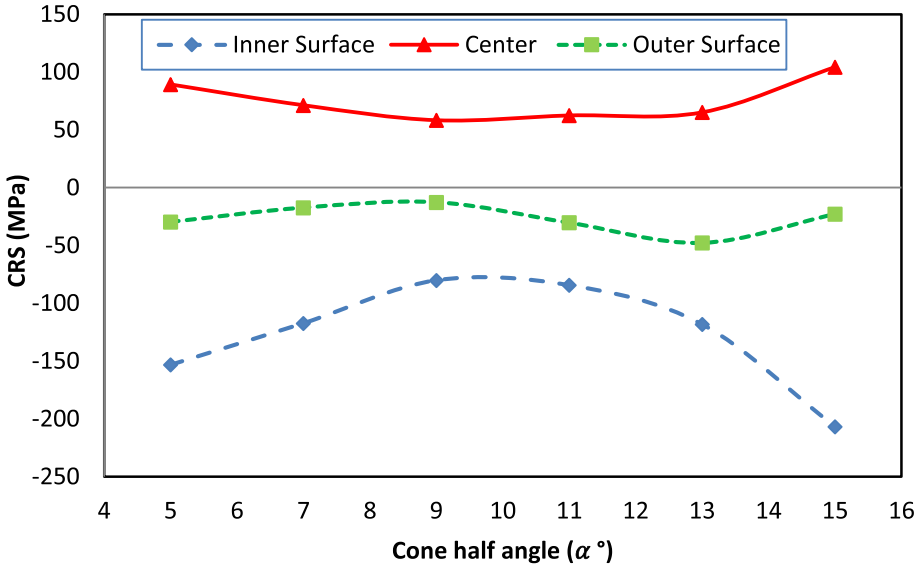


Fig. 14 Relationship between the CRS and cone half angle of the die (α °) by FEM

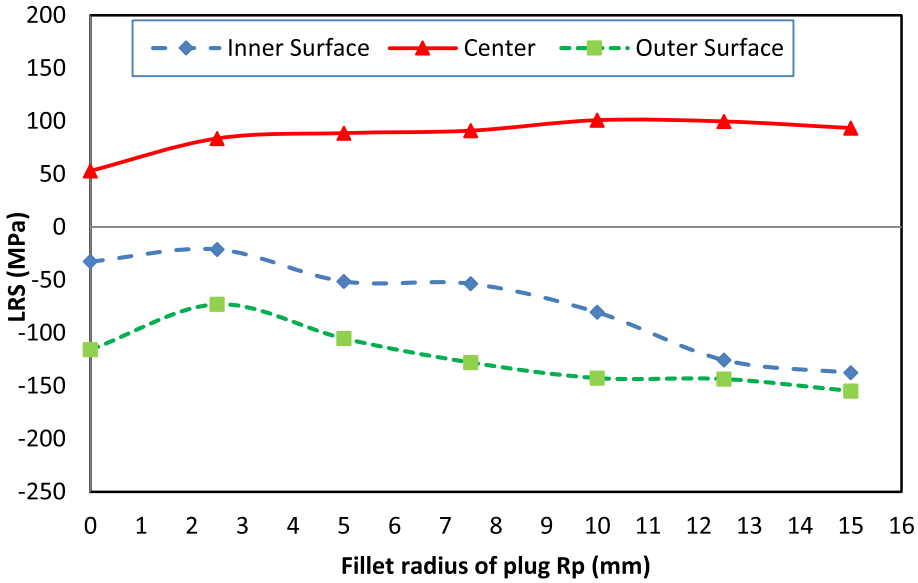


Fig. 15 Relationship between the LRS and fillet radius of plug (R_p) by FEM

depicted in Fig. 16, the LRS at the outer surface are completely compressive, while the CRS record compressive then tend to be tensile type R_p=12.5 to 15 mm. at to. Thus, it can be indicated that the most appropriate fillet radius of the plug can be selected within the range (0–10 mm) to obtain a compressive type of the IRS which prevent cracks propagation at the inner and the outer surfaces of the tube.

5.6 Effect of fillet radius of cone die on residual stresses

Figures 17 and 18 illustrate the results of the LRS and the CRS,respectively, which were determined by FEM at different fillet radius of die (R_d) with constant parameters, β=5°, α = 13° and R_p=0, and. It can be noticed that the LRS and the CRSare in a compressive behavior at the inner surface of the tube, while they are tensile at the center of the tube wall. Further, the LRS were a compressive type at the outer surface with various values of fillet radius. However, the CRSwere tensile type at ranges from 0 to 4 mm, and they were compressive type in the range of 5–15 mm. These figures indicate that choosing a fillet radius of the die between 7.5 and 10 mm increases the opportunity to obtain compressive residual stresses at the inner and the outer surface of the tube wall which in turn improve the quality of the product.

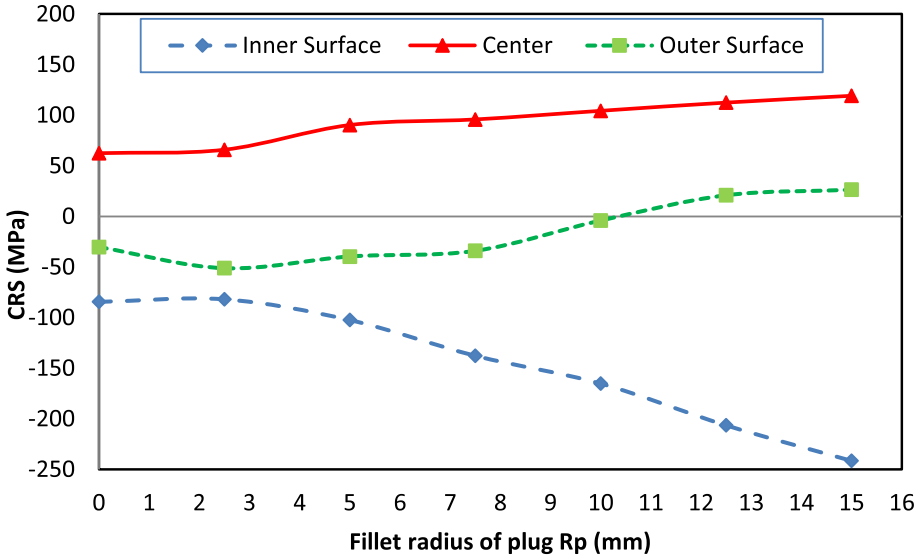


Fig. 16 Relationship between the CRS and fillet radius of plug (R_p) by FEM

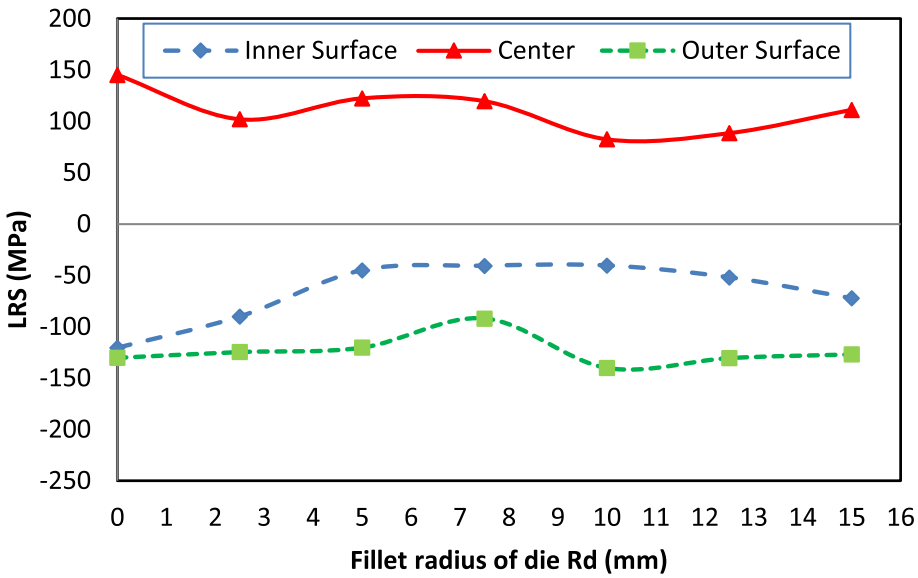


Fig. 17 Relationship between the LRS and fillet radius of die (R_d) by FEM

6 Conclusion

In this research, the cutting method was used to measure the induced residual stresses in the longitudinal and the circumferential directions within the tube wall of DIN 17,100 St 37–2 steel. The finite element method was employed to develop the models of tube drawing using a floating plug and to estimate the generated the LRS and the CRS after the drawing process. Effects of a floating plug and die geometry (the plug half angle, cone half angle of the die, fillet radius of the plug, and fillet radius of the die) on the IRS were investigated. The following results were drawn.

1. The results of both the CM and the FEM had good reliability although there was some discrepancy when comparing the two methods.
2. The performed tilting of tube walls from the pressure of the plug surface and cone surface of the die during the drawing process was responsible for determining the shape and value of the IRS inside the tube product.
3. The LRS and the CRS at different plug half angles and cone half angles of the die were compressive at the inner and the outer tube surfaces, while they were tensile at the center of the tube wall.

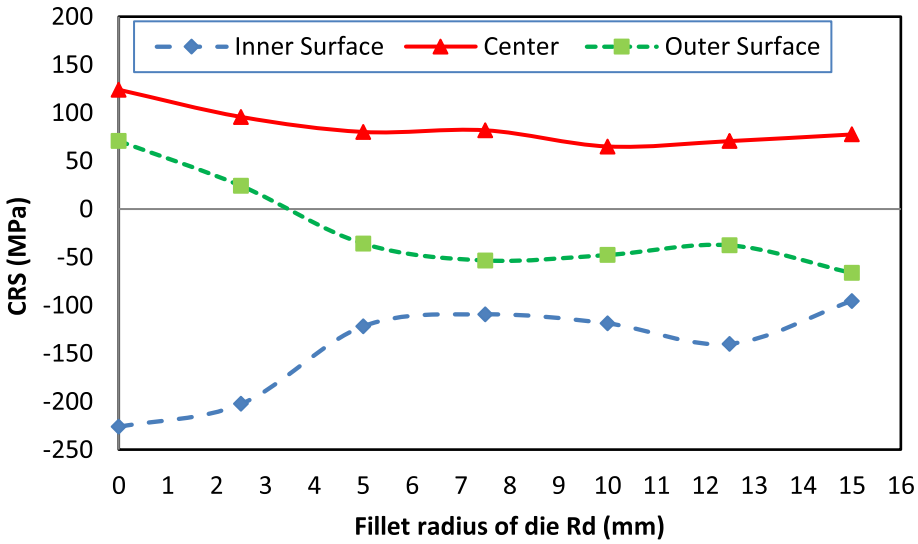


Fig. 18 Relationship between the CRS and fillet radius of die (R_d) by FEM

4. Plug half angle β=0°and cone half angle of the die α=9° resulted in a minimum values of the IRS compared to other selected ranges of angles.
5. The range of fillet radius of the plug (R_p=0–10 mm) and fillet radius of the die (R_d=7.50–10 mm) can be used to obtain compressive residual stresses that prevent cracks propagation toward the inner and the outer surface of the tube.

References

1. Guo W, Chen R, Jin J (2015) Online eccentricity monitoring of seamless tubes in cross-roll piercing mill. J Manuf Sci Eng 137:1–10. https://doi.org/10.1115/1.4028440
2. Gattmah J, Ozturk F, Orhan S (2016) Effects of the semi die/plug angles on cold tube drawing with a fixed plug by FEM for AISI 1010 steel tube. 4th International Symposium on Innovative Technologies in Engineering and Science. Turkey 2016:1065–1074
3. Bramley AN, Smith DJ (2013) Tube drawing with a floating plug. Met Technol 3(1):322–331. https://doi.org/10.1179/030716976803392277
4. Karanjule DB, Bhamare SS, Rao TH (2018) Determination of the optimal reduction ratio for least springback during cold drawing of seamless tubes. J Appl Comput Mech 4:275–285
5. Sheu J-J, Lin S-Y, Yu C-H (2014) Optimum die design for single pass steel tube drawing with large strain deformation. Proc Eng 81:688–693. https://doi.org/10.1016/j.proeng.2014.10.061
6. Patil M, Singh V, Simhachalam B, Srinivas K (2020) Effect of lubrication technique in tube drawing. Mater Today: Proc 28:426–431. https://doi.org/10.1016/j.matpr.2019.10.027
7. Heidariana F, Palkowski H (2020) Predicting the eccentricity of tubes by developing a multiple regression model in tube drawing process with tilted die. Proc Manuf 50:69–73. https://doi.org/10.1016/j.promfg.2020.08.013
8. Schrek A, Brusilová A, Švec B et al (2020) Analysis of the drawing process of small-sized seam tubes. Metals 10:1–20. https://doi.org/10.3390/met10060709
9. Chobaut N, Drezet J-M, Mischler S et al (2019) Miniaturized tube fixed plug drawing: determination of the friction coefficients and drawing limit of 316 LVM stainless steel. J Mater Process Technol 263:396–407. https://doi.org/10.1016/j.jmatprotec.2018.08.037
10. Bella P, Durcik R, Ridzon M et al (2018) Numerical simulation of cold drawing of steel tubes with straight internal rifling. Proc Eng 15:320–326. https://doi.org/10.1016/j.promfg.2018.07.225
11. Necpa M, Hodúlová E, Martinkovič M (2020) Numerical simulation of material plastic deformation using the drawing forming process of contoured internal surface tubes. Key Eng Mater 841:54–58. https://doi.org/10.4028/www.scientific.net/KEM.841.54
12. Boutenel F, Delhomme M, Velay V et al (2018) Finite element modelling of cold drawing for high-precision tubes. Comptes Rendus Mécanique 346:665–677. https://doi.org/10.1016/j.crme.2018.06.005
13. Hosseinzadeh M, Mouziraji MG (2016) An analysis of tube drawing process used to produce squared sections from round tubes through FE simulation and response surface methodology. Int J Adv Manuf Technol 87:2179–2194. https://doi.org/10.1007/s00170-016-8532-5
14. Ishkina SO, Charni D, Herrmann M et al (2021) Development of residual stresses by infeed rotary swaging of steel tubes. Arch Appl Mech 91:3637–3647. https://doi.org/10.1007/s00419-021-01905-5
15. Dorfmann L, Ogden RW (2021) The effect of residual stress on the stability of a circular cylindrical tube. J Eng Math. https://doi.org/10.1007/s10665-021-10097-4
16. Maier D, Stebner S, Ismail A et al (2021) The influence of free-form bending process parameters on residual stresses for steel tubes. Adv Ind Manuf Eng 2:100047. https://doi.org/10.1016/j.aime.2021.100047
17. Gattmah J, Ozturk F, Orhan S (2020) A new development of measurement technique for residual stresses generated by the cold tube drawing process with a fixed mandrel. Int J Adv Manuf Technol 108:3675–3687. https://doi.org/10.1007/s00170-020-05645-8
18. Yan X, Yang C (2019) Experimental research and analysis on residual stress distribution of circular steel tubes with different processing techniques. Thin-Walled Struct 144:106268. https://doi.org/10.1016/j.tws.2019.106268

19. Georgy S (2019) Experiment for determination of residual stresses in pipes. XIX International scientific-technical conference. The Ural schoolseminar of metal scientists-young researchers. KnE Eng 1:135
20. Kechout K, Amirat A, Zeghib N (2019) Residual stress analyses in multilayer PP/GFP/PP composite tube. Int J Adv Manuf Technol 103:4221–4231. https://doi.org/10.1007/s00170-019-03843-7
21. Foadian F, Carrado A, Brokmeier HG et al (2018) Integrated computational material engineering model development for tube drawing process. Proced Manuf 15:287–293. https://doi.org/10.1016/j.promfg.2018.07.221
22. Rozenbaum MA, Serebryakov AV, Serebryakov I et al (2017) Study of residual stresses and surface hardening in tubes for nuclear steam generators. Solid State Phenom 265:53–59. https://doi.org/10.4028/www.scientific.net/SSP.265.53
23. Lothhammer LR, Viotti MR, Veiga CLN et al (2017) Experimental evaluation of residual stresses in pipes manufactured by UOE and ERW processes. Exp Mech 57:287–296. https://doi.org/10.1007/s11340-016-0219-1
24. Gattmah J, Ozturk F, Orhan S (2017) Experimental and finite element analysis of residual stresses in cold tube drawing process with a fixed mandrel for AISI 1010 steel tube. Int J Adv Manuf Technol 93:1229–1241. https://doi.org/10.1007/s00170-017-0583-8
25. Linardon C (2006) Precision tube drawing for biomedical applications: Theoretical, Numerical and Experimental study. Dissertation, University of Grenoble
26. AZO materials (2002) Tungsten Carbide - An Overview https://www.azom.com/properties.aspx?ArticleID=1203
27. Liu Y (2010) Designation: E8/E8M – 09 Standard Test Methods for Tension Testing of Metallic Materials. https://www.academia.edu/14298711/Designation_E8_E8M_09_Standard_Test_Methods_for_Tension_Testing_of_Metallic_Materials
28. Pawtucket Ed (2013) ABAQUS 6.12 user's manuals, Hibbitt, Karlesson, and Sorensen, Inc.
29. Evin E, Daneshjo N, Mareš A et al (2021) Experimental assessment of friction coefficient in deep drawing and its verification by numerical simulation. Appl Sci 11:2756. https://doi.org/10.3390/app11062756
30. Abdin A, Feyzabi K, Hellman O et al (2018) Methods to create compressive stress in high strength steel components. Uppsala Universitet 1–52.

Publisher's Note Springer Nature remains neutral with regard to jurisdictional claims in published maps and institutional affiliations.